www.acsnano.org

Synthesis of Colloidal GaN and AlN Nanocrystals in Biphasic Molten Salt/Organic Solvent Mixtures under High-Pressure Ammonia

Wooje Cho, Zirui Zhou, Ruiming Lin, Justin C. Ondry, and Dmitri V. Talapin*



Downloaded via UNIV OF CHICAGO on January 2, 2024 at 22:41:16 (UTC). See https://pubs.acs.org/sharingguidelines for options on how to legitimately share published articles.

Cite This: ACS Nano 2023, 17, 1315-1326



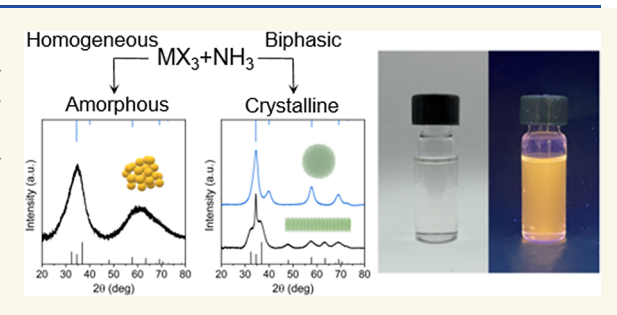
ACCESS I

Metrics & More

Article Recommendations

Supporting Information

ABSTRACT: Group III nitrides are of great technological importance for electronic devices. These materials have been widely manufactured via high-temperature methods such as physical vapor transport (PVT), chemical vapor deposition (CVD), and hydride vapor phase epitaxy (HVPE). The preparation of group III nitrides by colloidal synthesis methods would provide significant advantages in the form of optical tunability via size and shape control and enable cost reductions through scalable solution-based device integration. Solution syntheses of III-nitride nanocrystals, however, have been scarce, and the quality of the synthesized products has been



unsatisfactory for practical use. Here, we report that incorporating a molten salt phase in solution synthesis can provide a viable option for producing crystalline III-nitride nanomaterials. Crystalline GaN and AlN nanomaterials can be grown in a biphasic molten-salt/organic-solvent mixture under an ammonia atmosphere at moderate temperatures (less than 300 °C) and stabilized under ambient conditions by postsynthetic treatment with organic surface ligands. We suggest that microscopic reversibility of monomer attachment, which is essential for crystalline growth, can be achieved in molten salt during the nucleation and the growth of the III-nitride nanocrystals. We also show that increased ammonia pressure increases the size of the GaN nanocrystals produced. This work demonstrates that use of molten salt and high-pressure reactants significantly expands the chemical scope of solution synthesis of inorganic nanomaterials.

KEYWORDS: nanoparticle, solution synthesis, molten salt, high-pressure, group III-nitride

allium nitride (GaN) is a major semiconductor material for blue light-emitting diodes, lasers, and high-power and high-frequency electronic devices owing to its wide band gap, chemical stability, high breakdown electric field, and high electron saturation velocity. 1-3 Aluminum nitride (AlN) is another important group-III nitride material with intriguing properties such as an unusually strong ionicity of chemical bonds, very large absolute free energy of formation, a wide 6.0 eV bandgap, high thermal conductivity, and piezoelectricity. 3-5 Owing to these characteristics, AlN is used in optoelectronic devices, 6,7 high-power electronics, and microelectromechanical systems. As AlN and GaN are isostructural, they can form solid solutions (i.e., Al_xGa_{1-x}N), and important heterostructures such as quantum wells have been prepared with this materials system. 10

Various methods have been developed to grow GaN and AlN bulk crystals in melts, solutions, fluxes, and supercritical ammonia.^{3,11–21} III-nitride films have been grown on various substrates by vapor phase growth including physical vapor

transport (PVT), metal organic chemical vapor deposition (MOCVD), molecular-beam epitaxy (MBE), and hydride vapor phase epitaxy (HVPE).^{3,11,12} GaN and AlN with quasi one-dimensional (1D) structures such as nanorods, nanotubes, or nanocones have been produced through chemical vapor deposition (CVD), MBE, and template-assisted confined growth and their optoelectronic properties have been examined.^{13–19} Thin two-dimensional (2D) GaN crystals have also been synthesized by encapsulated growth within the narrow gap between graphene and silicon carbide (SiC)

Received: September 26, 2022 Accepted: December 23, 2022 Published: January 9, 2023





and by surface-confined nitridation reaction on liquid metal. 20,21

Colloidal semiconductor nanocrystals can demonstrate size-dependent optical and electronic properties. In small nanocrystals, the quantum confinement of electron and hole wave functions enables fine-tuning of electronic structures *via* size and shape engineering. Colloidal nanomaterials offer a way to incorporate semiconductors into nonepitaxial thin-film devices (LEDs, displays, light detectors, *etc.*) using inexpensive solution-based processing and patterning. Importantly, group III nitrides do not incorporate rare or toxic elements and do not release highly toxic gases upon decomposition, which is rare among III—V and most other semiconductors. However, little work has been published on solution synthesis of colloidal GaN and AlN nanomaterials compared to the enormous body of work on II—VI semiconductors or on group III phosphide and arsenide semiconductors.

Sardar et al. reported the solvothermal reaction of galliumcupferron complex or gallium chloride with hexamethyldisilazane in toluene.²³ Another bimolecular synthesis was recently reported by Choi et al. using gallium stearate and lithium bis(trimethylsilyl)amide in 1-octadecene solvent.²⁴ There are also reports on synthetic routes using thermal decomposition of molecular or polymeric precursors. Manz et al. found that molecular gallium azide can thermally decompose in triglyme solvent at 216 °C in 24 h. Unfortunately, the particles were not sufficiently crystalline to provide X-ray diffraction data.²⁵ Mićić et al. reported the synthesis of GaN nanoparticles by pyrolysis of poly(imidogallane).²⁶ The method required long reaction times (>48 h) and produced only a low yield of colloidal particles. The method was later improved by Pan et al. using dimeric bis(dimethylamido)gallium to produce a higher yield of colloidal particles in a shorter reaction time (24 h).²⁷ All these syntheses produced GaN nanoparticles, but their qualities (crystallinity, defects, surface passivation, colloidal stability, and size monodispersity) have not been on par with those of established II-VI (e.g., CdSe), IV-VI (e.g., PbS), and III-V (e.g., InP) quantum dot materials successfully used for device applications.

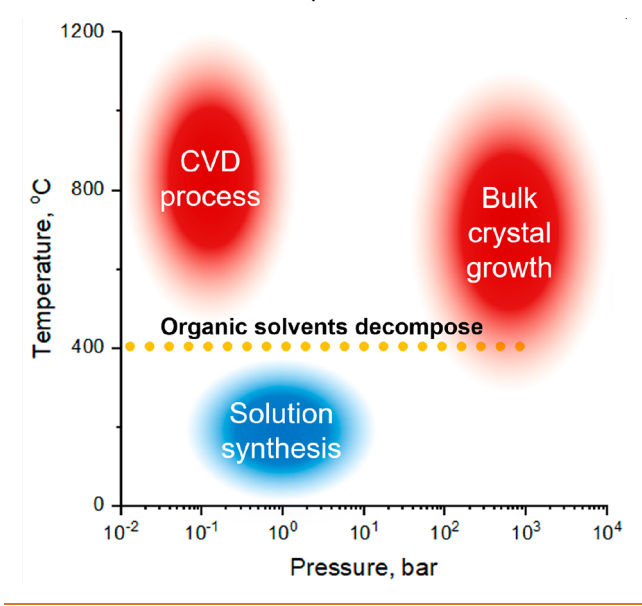
Reports of solution syntheses of AlN nanoparticles are even more limited. Lan *et al.* reported an ammonothermal method involving heating Al metal and ammonium chloride at 450 °C for 2 days.²⁸ Sardar *et al.* reported a solvothermal reaction of aluminum-cupferron complex or aluminum chloride with hexamethyldisilazane in toluene similar to their GaN synthesis²³ but at a higher temperature of 350 or 450 °C.²⁹ These two methods produced some AlN nanoparticles but with very limited control over size, shape, and colloidal stability. AlN synthesis at lower temperature (110 °C) was reported by Lu *et al.* using aluminum chloride and lithium nitride, but the nanoparticles showed crystalline X-ray diffraction patterns only after annealing at 600 °C.³⁰

To date, a traditional colloidal nanoparticle synthesis, *via* controlled nucleation and growth from molecular precursors in solution phase, has been unable to produce GaN and AlN nanocrystals with structural perfection, size, and shape control comparable to those produced by well-developed methods for preparing, *e.g.*, CdSe, InP, and CsPbBr₃ nanocrystals. This difficulty can be rationalized by taking into account the need for microscopic reversibility of monomer addition during the growth of crystalline particles.³¹ Irreversible formation of chemical bonds during crystal growth implies that the bonds cannot be efficiently rearranged after they are formed. This

inability to disassemble and reorganize incorrectly bonded fragments, which are inevitably formed during crystal growth, prevents formation of perfect crystals, so syntheses lacking microscopic reversibility typically result in highly defective or amorphous products rather than crystalline reaction products. The bond dissociation energies (BDEs) for Ga–N, Al–N, Cd–Se, and In–P bonds are 240, 268, 128, and 198 kJ/mol, respectively. Since GaN and AlN crystals incorporate much stronger bonds than CdSe or InP crystals, growing crystalline GaN and AlN nanostructures may require higher temperatures or other unusual conditions for achieving reversible bond formation.

A simple comparison of the optimized conditions for the CVD synthesis of GaN and AlN films, growth of bulk GaN and AlN crystals, and the parameter space accessible for traditional colloidal synthesis (Scheme 1) suggests that traditional

Scheme 1. Parameter Space Accessible for Traditional Solution Synthesis Compared to the Conditions Optimized for Chemical Vapor Deposition (CVD) and Bulk Crystal Growth of GaN and AlN Crystals and Films



solution synthesis of GaN and AlN nanostructures may be difficult to implement with currently used reaction setups, solvents, and surface ligands. Most CVD processes for GaN and AlN growth happen in the 500–1000 °C temperature range. 11,19 Other popular growth techniques for bulk GaN and AlN crystals require both high temperature and high pressure; e.g., 350–850 °C and 100–500 MPa have been used in the ammonothermal syntheses. 3,12 Solution synthesis, however, typically uses high-boiling organic solvents that chemically decompose above 400 °C. 4 Furthermore, typical laboratory glassware cannot access the pressure range previously identified suitable for growth of high-quality GaN crystals. These limitations suggest that different synthetic approaches are needed to achieve controllable solution synthesis of crystalline III-nitride materials.

Here, we report an approach to synthesize crystalline colloidal GaN and AlN nanostructures. We take advantage of a molten salt phase together with high-boiling organic solvents, somewhat similar to a synthetic system for CdSe nanoplatelet growth. The presence of a molten salt phase helps the III-nitride system to achieve microscopic reversibility at temper-

ACS Nano www.acsnano.org Article

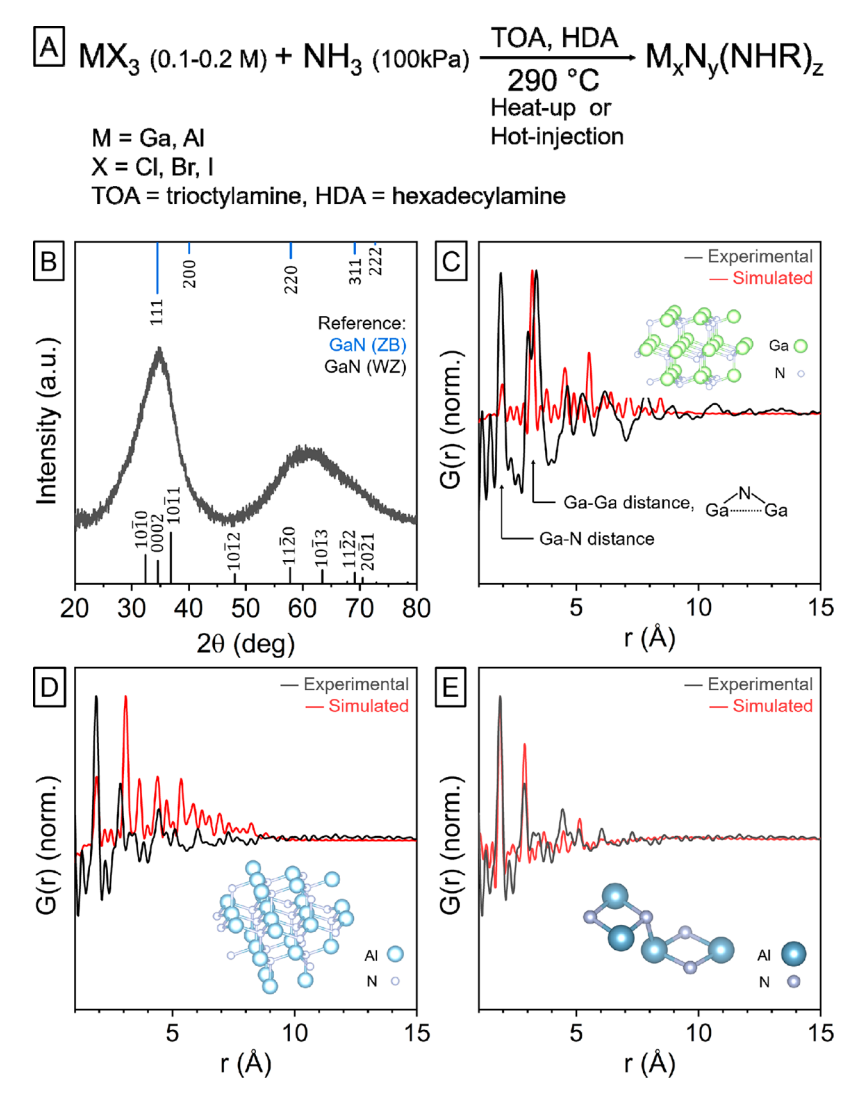


Figure 1. Reactions of 0.1–0.2 M gallium and aluminum halides with NH₃ at 290 °C in trioctylamine/hexadecylamine (TOA/HDA) solution. (A) The reaction scheme. (B) Powder X-ray diffraction (PXRD) pattern measured from the products of the reaction of 0.2 M GaCl₃ with excess NH₃ in TOA/HDA solution. The vertical lines show the positions and relative intensities for bulk zinc blende (ZB, blue vertical lines) and wurtzite (WZ, black vertical lines) GaN phases. (C) The atomic pair distribution function (PDF) measured for the products of the reaction between 0.2 M GaCl₃ and excess NH₃ in TOA/HDA solution. The experimental data (black line) are compared with the simulated PDF (red line) of a 1 nm-diameter wurtzite GaN nanocrystal (inset cartoon). (D and E) PDFs of the product of the reaction between 0.1 M AlBr₃ and excess NH₃ in TOA/HDA solution. Inset figures represent the structures used for simulations. The experimental data (black line) are compared with the simulated PDFs (red line) of a 1 nm-diameter spherical WZ AlN crystal (D) and a molecular 4-membered-ring AlN structure (E).

atures consistent with traditional colloidal syntheses. GaN nanorods, spherical GaN nanocrystals, and AlN nanorods were all prepared under mild conditions and demonstrated good colloidal stability in organic solvents. Additionally, we show that increasing the ammonia pressure from 0.1 to 5 MPa increases the diameter of GaN nanorods.

RESULT AND DISCUSSION

General Considerations for the Solution Synthesis of GaN and AlN. Solution synthesis offers a broad scope of precursors, surface ligands, and additives that can efficiently mediate precursor reactivity through tuning solvent polarity, redox potentials, pH, and other parameters. For colloidal synthesis of compound semiconductors, the metal source is usually a metal cation coordinated with long alkyl-chain ligands (e.g., Cd(oleate)₂, InCl₃-oleylamine complex, etc.). The chalcogenide or pnictide precursors are provided as reduced

species soluble in nonpolar solvents (*e.g.*, tri-*n*-octylphosphine selenide (TOPSe), tris(trimethylsilyl)phosphine [(CH₃)₃Si]₃P, *etc.*). A variety of metal precursors have been studied in solution syntheses of III–V nanocrystals including metal carboxylates and metal halides. ^{23–26,36–39} Indium and gallium carboxylates have been explored extensively for the synthesis of III–V nanocrystals, resulting in good control over size and size distribution. ^{24,36–39} However, we found that higher oxophilicity of Ga(III) species compared to In(III) creates a problem for the synthesis of phase-pure GaN nanocrystals. In our studies, gallium precursors containing Ga–O bonds easily introduced oxygen doping of GaN phase during the reaction. For example, the reaction of gallium stearate in trioctylamine solvent with thoroughly dried, oxygen-free ammonia at 290 °C produced gallium oxynitride spinel (Ga_{2.81}O_{3.57}N_{0.43}) rather than GaN (Figure S1). In fact, a careful inspection of reported powder X-ray diffraction (PXRD) patterns for GaN nano-

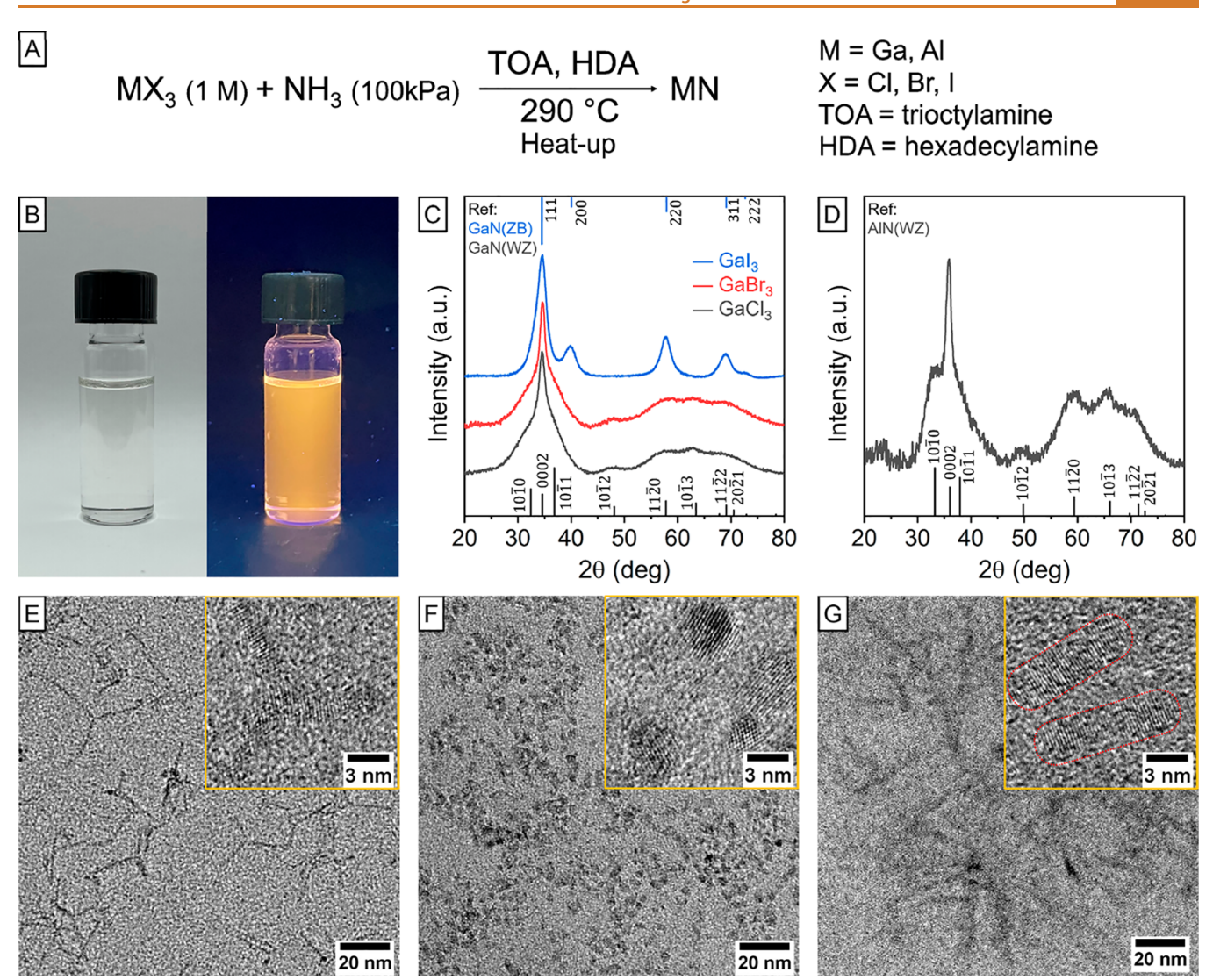


Figure 2. Solution synthesis of crystalline GaN and AlN nanomaterials. (A) The reaction scheme. (B) Photographs of a colloidal solution of GaN nanoparticles under ambient light (left) and under illumination with 302 nm ultraviolet (UV) light (right). Under UV, the solution glows yellow due to emissions from midgap states. (C) Powder XRD patterns of GaN nanocrystals synthesized by reacting NH₃ with GaCl₃ (black curve), GaBr₃ (red curve), and GaI₃ (blue curve) with reference lines from wurtzite (WZ, black vertical lines) and zinc blende (ZB, blue vertical lines) bulk GaN phases. (D) Powder XRD pattern of AlN nanorods synthesized from AlBr₃ (black curve) with reference lines from WZ AlN phase (vertical lines). (E) TEM image of WZ GaN nanorods and nanotetrapods synthesized using GaCl₃. The inset shows a high-resolution TEM image. (F) TEM image of ZB GaN nanocrystals synthesized using GaI₃. The inset shows a high-resolution TEM image. (G) TEM image of AlN nanorods. The inset shows a high-resolution TEM image. AlN nanorods are marked with dotted red lines.

crystals synthesized from gallium cupferron and stearate precursors 23,24 revealed a small peak at $\sim\!43^\circ$ 2θ angle (Cu K α source), which is not present in either wurtzite (WZ) or zinc blende (ZB) gallium nitride phases but typical for gallium oxynitrides. From these observations, we suspected that metal precursors used for GaN synthesis should not contain Ga–O bonds. The same is likely to be true for aluminum, as aluminum makes an even stronger bond with oxygen than gallium (BDE for Ga–O is 374 kJ/mol, while for Al–O it is 502 kJ/mol). Therefore, to avoid inclusion of oxygen impurities in GaN and AlN nanostructures, we used oxygen-free precursors, solvents, and other components of the reaction mixture.

Oxygen-free conditions can be realized by using metal halides, ammonia, and amines. These precursors have been successfully used for CVD synthesis of III-nitride materials. We studied the products of reactions between MX_3 (M = Ga,

Al; X = Cl, Br, I) and NH₃ in alkylamine solvent (Figure 1A). In a heat-up approach, 0.1 and 0.2 M solutions of MX₃ in 4 mL of freshly distilled trioctylamine (TOA) and 0.6 g of hexadecylamine (HDA) were heated from room temperature to 290 °C under a constant flow of ammonia. Alternatively, in a hot-injection approach, the MX3 solution was preheated to 290 °C under a dry nitrogen atmosphere, followed by the addition of flowing ammonia through the reaction flask for 5 min. The reaction mixture was kept at 290 °C for 1 h before cooling to room temperature. As-synthesized products in both approaches were noncolloidal at room temperature and could be separated from solution with centrifugation. The resulting white solids were washed with toluene to remove the remaining alkylamines and then with methanol to remove ammonium halides, a major byproduct of these reactions. All the reaction products of GaX₃ precursors showed similar PXRD patterns with two broad features around 35° and 60° 2θ

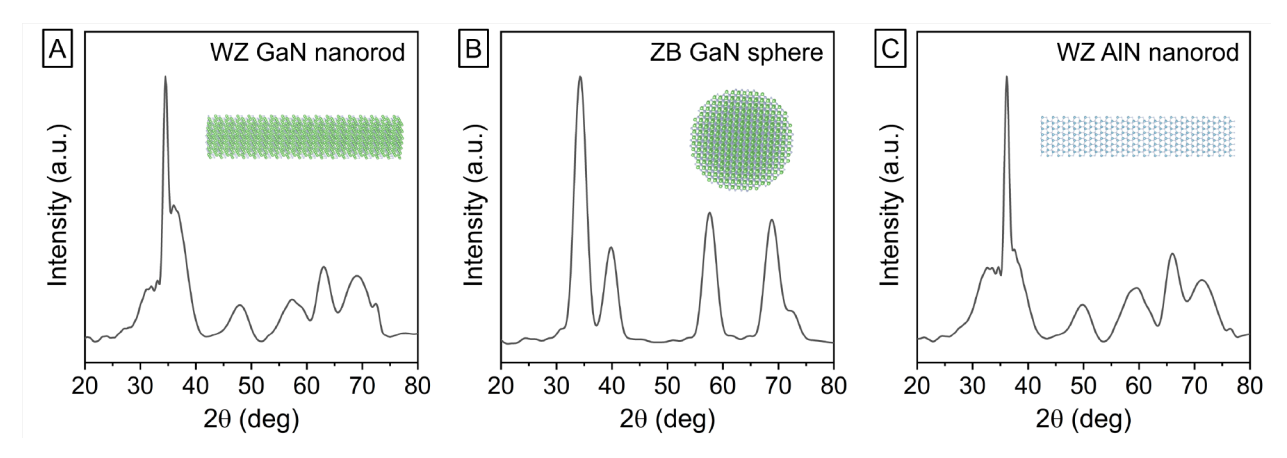


Figure 3. Simulated powder XRD patterns for different GaN and AlN nanomaterials: (A) WZ GaN nanorod with 2 nm diameter and 9 nm length, (B) spherical ZB GaN nanocrystal with 4 nm diameter, and (C) WZ AlN nanorod with 2 nm diameter and 9 nm length.

angles (Figure 1B and Figure S2). No obvious diffraction peaks were present in the PXRD pattern of a product of the reaction between ammonia and AlBr₃, implying the formation of an amorphous material (Figure S2).

To better understand the nature of the reaction products, we carried out X-ray atomic pair distribution function (PDF) analysis of the products formed by reacting 0.1 or 0.2 M MX₃ (M = Ga, Al; X = Cl, Br, I) solutions with excess NH_3 . Parts C-E of Figure 1 show the pair distribution functions, G(r), for the "GaN" and "AlN" reaction products. We compared our experimental data with the simulated G(r) from GaN and AlN nanocrystals. For the GaCl3+NH3 reaction products, the interatomic distances for the first two G(r) peaks are close to the positions expected for crystalline GaN, but the peaks at larger distances significantly deviate from the interatomic distances in a GaN crystal (Figure 1C). The first G(r) peak reflects Ga-N bonds, which is slightly shorter (1.90 Å) than the expected distance in GaN crystals (1.95 Å). The second G(r) peak reflects the nearest Ga···Ga distances, and these distances match well to the expected value in GaN crystals, which implies that Ga-N-Ga bond angles are close to 109.5° expected for tetrahedral coordination. The second peak splits into two components, suggestive of two distinct bonding motifs. Moreover, the ratio of intensities for the first two G(r)peaks corresponding to Ga-N and Ga-Ga distances in our reaction product is significantly larger than that ratio for crystalline GaN. This discrepancy suggests that many nitrogen atoms forming Ga-N bonds do not participate in the bridging Ga-N-Ga bonding. A shorter Ga-N bond length, broader features from Ga...Ga correlations, and suppressed intensities for the peaks from longer-distance atomic pairs are predicted to be the characteristics of amorphous GaN. 41 Taken together, our PDF analysis concludes that the GaCl₃+NH₃ reaction product is an amorphous material consisting of distorted tetrahedral structures with numerous Ga vacancies, which only locally resembles the tetrahedrally coordinated crystalline phase.

Based on the PDF analysis, the AlBr₃+NH₃ reaction product has a totally different structure than its gallium counterpart. Except for the first peak (Al–N bonds, ~ 1.90 Å), all other G(r) features significantly deviate from those expected for AlN crystals (Figure 1D). The AlBr₃+NH₃ reaction did not yield a product adopting any motif of the WZ or ZB structures. The second G(r) peak, corresponding to the nearest Al···Al distance (2.87 Å), significantly deviates from the Al···Al

distance in WZ or ZB AlN (3.08 Å). A rapid decay of G(r) amplitude also suggests the formation of small molecular fragments with no long-range correlations. We suggest that experimental G(r) data can best be described as polymeric structures incorporating Al_2N_2 four-membered rings. There are numerous prior reports of small molecules and short chains with an $Al-(\mu_2-NR)_2$ -Al four-membered ring structural motif. The Al-N-Al bond angle calculated from the positions of first two G(r) peaks is also consistent with this assignment (Figure 1E).

The noncrystalline nature of MX₃+NH₃ reaction products can result from the irreversible binding of metal and nitrogen containing fragments with no subsequent rearrangements of subunits. In contrast, the formation of GaN and AlN crystals requires microscopically reversible binding of the atomic building blocks.³¹ Traditional CVD synthesis of III-nitrides approaches microscopic reversibility of GaN and AlN growth by using high temperatures. Unfortunately, solution methods do not permit arbitrarily increasing reaction temperature due to solvent decomposition. This may be one reason, despite the great success of CVD-grown nitride semiconductors, there has only been limited progress with the solution synthesis of GaN and AlN nanomaterials.

Formation of Crystalline GaN and AlN Nanostructures in Solution. We found that crystalline GaN and AlN nanostructures could be synthesized if the reaction between Ga or Al halides and ammonia was carried out in the reaction mixture containing higher concentrations of metal halide precursors, nominally exceeding 1 M GaX3 or AlX3 in TOA and HDA (Figure 2A). In a typical synthesis, 5 mmol of finely ground anhydrous metal halide salt was mixed with 4 mL of TOA and 0.6 g of HDA, and then, ammonia was passed over the mixture at room temperature, followed by heating to 290 °C. The reaction mixture was held at 290 °C for 1 h and then cooled to room temperature. The resulting III-nitride particles were not colloidal at this stage and were collected with centrifugation. The solid was washed first with toluene and then methanol to remove excess alkylamines and ammonium halide, respectively. The nanoparticles could then be colloidally stabilized in an *n*-hexane or toluene solution of oleylamine and oleic acid (10% v/v each) after brief sonication. The remaining noncolloidal part was removed by centrifugation, and nanoparticles in the supernatant were flocculated with ethanol followed by dispersion in fresh *n*-hexane or methylcyclohexane to form a colloidal solution (Figure 2B). The entire process of

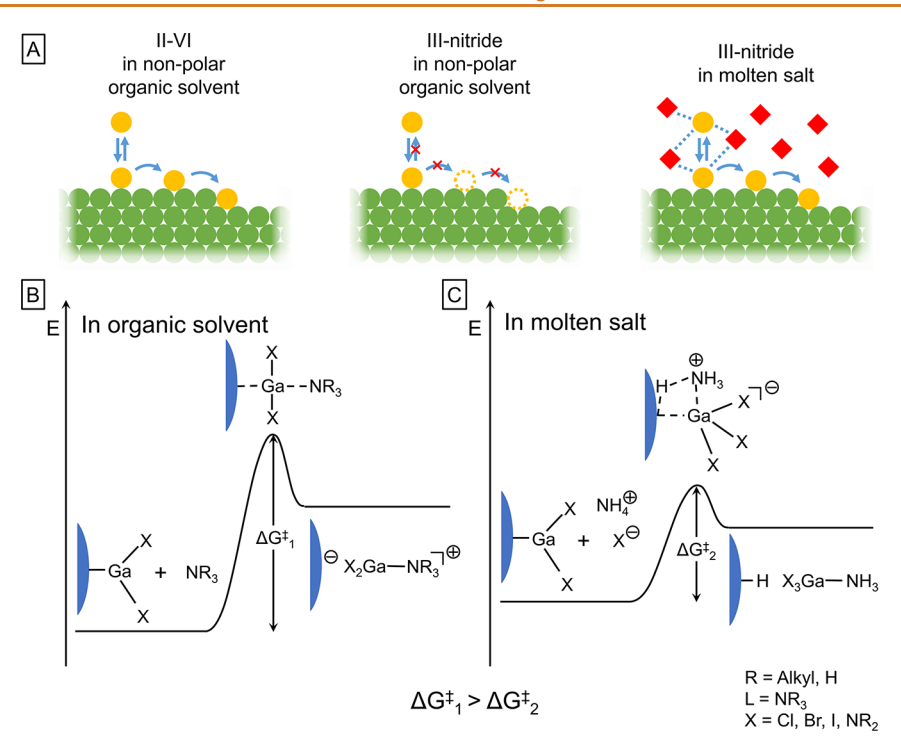


Figure 4. Molten salt enables solution synthesis of crystalline III-nitride nanocrystals by facilitating microscopic reversibility of crystal growth. (A) Cartoons depicting microscopic reversibility during synthesis of II-VI and III-nitride nanocrystals. Yellow circles represent monomers of the corresponding system, and red squares illustrate ions in molten salts. (B) The free energy landscape for the elementary step of breaking Ga-N surface bonds required for establishing microscopic reversibility. A highly polarizable molten salt medium facilitates rearrangement of surface Ga-N bonds during nanocrystal growth.

synthesis and purification was conducted under an inert atmosphere; this is necessary during synthesis to avoid oxygen inclusion and is highly recommended during purification, as the III-nitride particles slowly lose their colloidal stability upon exposure to air.

Gallium chloride and gallium bromide precursors yielded highly anisotropic WZ-phase GaN nanostructures, grown along the [0001] crystallographic direction, which included nanotetrapods and nanorods (Figure 2C,E and Figure S3). Their PXRD patterns showed sharp (0002) peaks in agreement with simulated X-ray diffraction patterns for nanorods of WZ GaN phase (Figures 2C and 3A). TEM images indicated that the products from reactions using gallium chloride had a higher proportion of nanotetrapods than those from gallium bromide reactions (Figure 2E and Figure S3). TEM images also revealed that the product from gallium bromide reactions had tiny spherical nanocrystals, which were not noticeable in PXRD patterns, mixed with the nanorods. When gallium iodide was used as the precursor, spherical ZB-phase GaN nanocrystals formed instead of WZ GaN nanorods (Figure 2C,F). The Scherrer grain size of the spherical ZB GaN particles was about 4 nm, and the PXRD pattern matched well with the simulated pattern (Figure 3B).

X-ray PDF analysis of the nanocrystalline reaction products was also performed for direct comparison with the amorphous GaN products (Figure S4). The importance of combined PXRD and PDF studies can be highlighted on the examples of the reaction products of 1 M GaCl₃ and GaBr₃ with NH₃. The reaction products for both reactions showed similar PXRD patterns (Figure 2C), but PDF data revealed that GaCl₃ reaction product contained significant amounts of amorphous byproducts, similar to what was discussed in the previous section (Figure 1C and Figure S4A). PDFs of products from

gallium bromide and gallium iodide reactions match well with expected patterns from simulated nanocrystalline GaN in WZ and ZB phases, respectively (Figure S4B,C). It is notable that PDFs of GaN nanocrystals from gallium bromide showed periodic correlations up to 5 nm interatomic distance (Figure S4E). The correlation has a period of 0.26 nm, which is the distance between [0002] planes of WZ-GaN crystal, hinting that nanocrystals grew anisotropically along the [0001] direction, in agreement with the narrow (0002) PXRD peak.

The reaction of 1 M AlBr $_3$ with NH $_3$ also produced WZ AlN nanorods grown along the [0001] direction, showing a sharp (0002) peak in PXRD, in line with the patterns observed for GaN nanorods (Figures 2D,G and 3C). Unfortunately, the yield of AlN nanorods versus amorphous AlN byproducts varied from run to run, and the conditions for synthesis of AlN nanocrystals of various sizes and shapes are yet to be optimized.

The formation of crystalline GaN and AlN particles is counterintuitive because using the same MX₃ and NH₃ precursors yielded amorphous products when the halide salt was present at lower concentrations (cf. Figure 1 and Figure S2). A careful inspection of the reaction conditions showed that the most notable difference among the experimental runs producing crystalline versus amorphous products was homogeneity of the reaction mixture. Crystalline particles formed when we used large amounts of GaX₃ or AlX₃ salts and when the halide salts were not fully dissolved in TOA/HDA solvent before the reaction started. Due to low melting points of gallium and aluminum halides (77.9 °C for GaCl₃, 121.5 °C for GaBr₃, 212 °C for GaI₃, and 97.5 °C for AlBr₃), the reaction mixtures contained a molten inorganic salt phase immiscible with the organic phase. This molten salt phase likely plays an

important role in the formation of crystalline GaN and AlN phases, as discussed below.

The reaction between GaX₃ and NH₃ generated fine white solids of ammonium halide and III-nitride products that obscured direct observation of molten gallium halide droplets during the reaction. Therefore, we aimed to determine whether this inhomogeneity was indeed required for the synthesis of crystalline particles or crystallization was simply induced by an increased salt concentration. While gallium chloride is soluble in the mixture of TOA and HDA at high temperature, potassium tetrachlorogallate (KGaCl₄) remains phase-separated from TOA/HDA mixtures at 250 °C, which is above the melting point of KGaCl₄ (Figure S5). Hot injection of excess ammonia into a homogeneous solution containing 1 mmol of GaCl₃ in 4 mL of TOA and 0.6 g of HDA preheated to 290 °C resulted in amorphous reaction products (Figure S6). The hot injection of excess ammonia into a biphasic mixture of 1 mmol of KGaCl₄, 4 mL of TOA, and 0.6 g of HDA at 290 °C resulted in a qualitatively different reaction product (Figure S6). A homogeneous solution of gallium chloride generated only amorphous species, similar to those described in Figure S2, while the biphasic mixture of KGaCl₄ produced crystalline WZ-GaN nanorods. Therefore, it appears plausible that the molten salt phase is required to generate crystalline III-nitride nanomaterials.

As described previously, microscopic reversibility during nucleation and growth is essential to generate crystalline particles. Figure 4A schematically illustrates monomer additions to a growing nanoparticle in different material systems. In a synthesis of II—VI (e.g., CdSe) nanocrystals, monomer additions are reversible due to relatively small chemical bond energy, and, therefore, the growth of a crystalline phase can occur at relatively low temperatures via reversible addition of atoms (Figure 4A, left panel). Unlike II—VI semiconductors, GaN and AlN have strong bonds that impede efficient formation of crystalline products in organic solution (Figure 4A, middle panel). However, our results suggest that the presence of molten salts in the reaction mixture can restore the microscopic reversibility during nucleation and growth (Figure 4A, right panel).

Establishing microscopic mechanism to explain the effect of molten salt on GaN and AlN nanocrystal synthesis requires further investigation. We suggest that the molten salt environment facilitates monomer detachment by efficiently stabilizing charged species. Parts B and C of Figure 4 schematically depict possible pathways for surface atom detachment with cleavage of Ga-N bonds. For a typical ZB or WZ III-V nanocrystal terminated with thermodynamically stable low-index facets, surface metal atoms can be bonded to two X-type ligands, which can be represented as Z-type GaX₂ fragment. 43,44 In nonpolar organic solvents, charged species are energetically unfavorable and chemical species typically remain charge-neutral. A detachment of the surface Ga atom likely proceeds via L-promoted Z-type ligand displacement⁴³ where nucleophilic L-type ligand (alkylamine) binds to the surface Ga atom and weakens its bonding with the crystal lattice (Figure 4B). Such cleavage generates charged species, and the energy of the system is greatly increased. However, in a highly polarizable molten salt environment, charged species are present in large quantities. The removal of a Z-type GaX2 group can be promoted by an X-type anion, followed by a proton transfer from an ammonium ion to negatively charged surface nitrogen site (Figure 4C). This process, nominally X-

promoted Z-type ligand displacement, does not produce any highly unstable charged nor undercoordinated reaction products, and the energy change of the system is moderate. The detachment of misbound surface atoms can therefore occur more efficiently in molten salts compared to nonpolar organic solvents, which are typically used for nanocrystal synthesis.

There are considerable precedents that molten salt phases encourage the formation of crystalline phases at lower temperatures in flux-based solid state synthesis. 45,46 Also, the presence of molten salt byproducts in solid state metathesis reactions is suspected to be important for obtaining crystalline materials. 47,48 In colloidal nanocrystal synthesis, there are experimental and computational evidence that molten salt droplets of cadmium acetate can serve as the nucleation and growth media during synthesis of two-dimensional ZB CdS, CdSe, or CdTe nanoplatelets.³⁵ High concentrations of the reagents in molten salt result in reaction-rate-controlled rather than diffusion-controlled kinetics of nucleation and growth.³⁵ The same argument may explain the formation of anisotropic WZ III-nitride nanocrystals, because one-dimensional nanorods and two-dimensional nanoplatelets can form through a very similar reaction-rate-limited pathway. 49 It has been also reported that high monomer concentration causes WZ CdSe particles to become rods rather than spheres. 50 However, the monomer concentration alone cannot explain the formation of spherical ZB GaN nanocrystals. The effect of halide ions on surface energy of different nanocrystal facets may be an alternative explanation for the shape and phase of our reaction products. It has been shown that different halide additives can affect the shapes and the phases of nanocrystals for other systems. 51-53

Solution Synthesis of III-Nitride Nanostructures Using High-Pressure Ammonia. The growth of bulk GaN crystals is typically carried out using high-pressure ammonia, often under supercritical conditions. 3,12 To test the effect of ammonia pressure on the colloidal synthesis of III-nitride nanocrystals, we developed a system for running solution phase reactions under high-pressure ammonia gas. A mixture of 5 mmol of KGaCl₄, 4 mL of TOA, and 0.6 g of HDA was contained in a silicon nitride liner and preheated to 290 °C in a stainless-steel pressure vessel. High-pressure ammonia was prepared by heating predried liquid ammonia in a separate pressure vessel. The two pressure vessels were connected, and high-pressure ammonia of 2, 3.5, or 5 MPa was transferred to the reaction vessel. As the case of ambient pressure GaN synthesis, after heating for 1 h at 290 °C, the vessels were cooled to room temperature. As an ambient-pressure (100 kPa) control, the reaction mixture containing the same amounts of KGaCl₄, TOA, and HDA was preheated to 290 °C, followed by a flow of ambient-pressure ammonia for 5 min. This mixture was maintained for 1 h at 290 °C and then cooled to room temperature. In all cases, as-synthesized particles did not form stable colloidal dispersions and could be collected by centrifugation. Precipitates were washed first with toluene to remove excess alkylamines and then with methanol to remove salt byproducts. A brief sonication with oleylamine and oleic acid (10% v/v each) in n-hexane or toluene stabilized the GaN nanocrystals as a colloidal solution. After removal of the remaining solids by centrifugation, GaN nanocrystals were flocculated with ethanol from colloidal solution and redispersed in fresh *n*-hexane or methylcyclohexane.

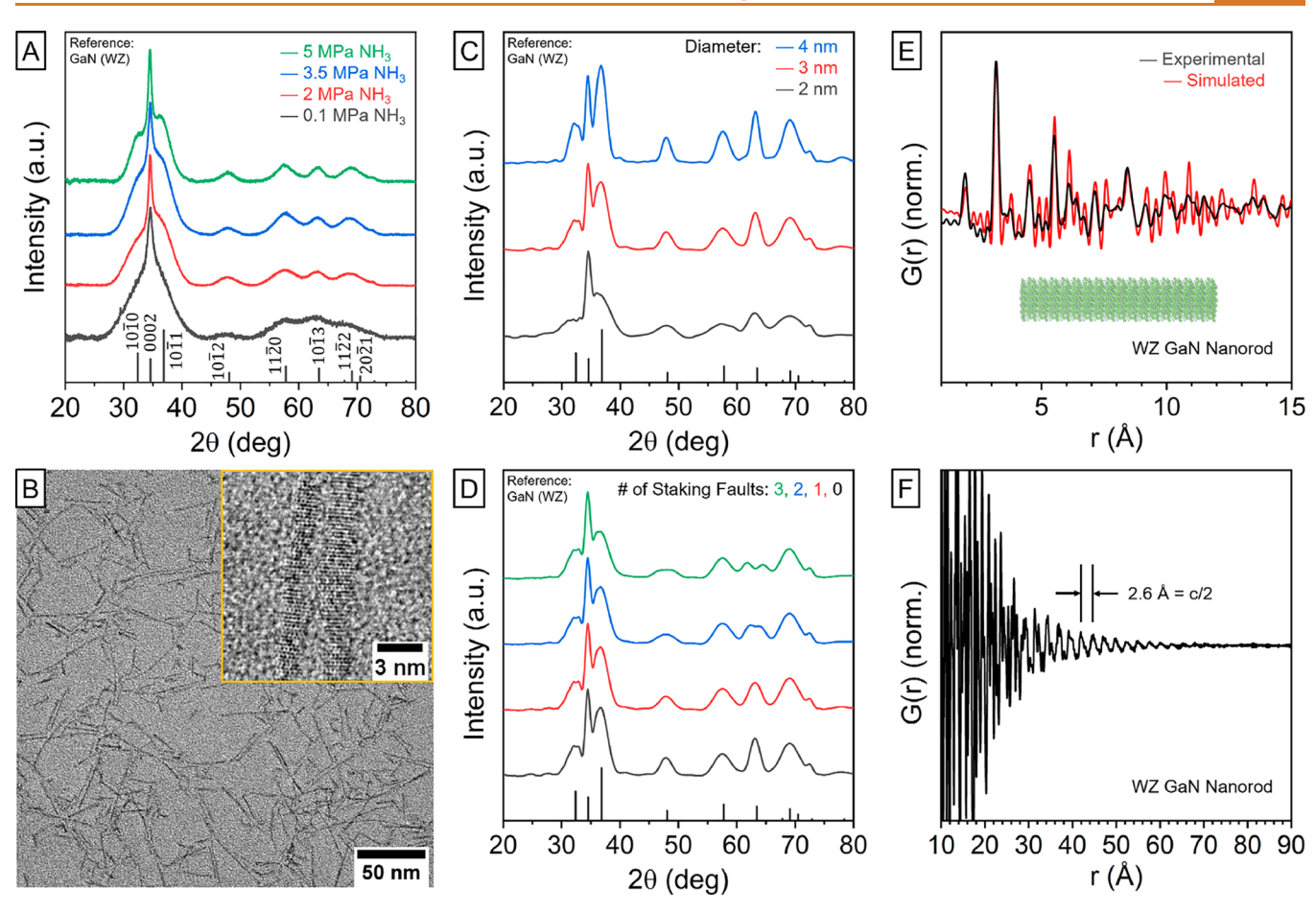


Figure 5. GaN nanorods synthesized using high-pressure ammonia. (A) PXRD patterns of GaN nanorods produced using different ammonia pressures. Black vertical lines correspond to a WZ GaN reference. (B) TEM image of GaN nanostructures synthesized using 5 MPa ammonia. The inset shows a high-resolution TEM image of GaN nanorods. (C and D) Simulated PXRD patterns of WZ GaN nanorods with different thicknesses (C) and different numbers of stacking faults (D). (E and F) PDF pattern of GaN nanorods synthesized with ammonia at 5 MPa. (E) Shorter range data (black line) in pair with a simulated PDF pattern (red line) from WZ GaN nanorod with 2 nm diameter and 9 nm length (inset cartoon). (F) Longer range PDF reveals [0002] planes of WZ GaN.

While GaN nanorods were formed regardless of ammonia pressure, a clear difference between the reaction products synthesized using ambient-pressure ammonia and highpressure ammonia was observed in PXRD patterns and in the absorption spectra (Figures 5A and 6A). Generally, the diameter of GaN nanorods increased as the ammonia pressure increased. The X-ray diffraction peaks became significantly narrower for nanorods grown at higher ammonia pressures (Figure 5A). This trend agreed with our simulated PXRD patterns of WZ-GaN nanorods with different thicknesses (Figure 5C). PXRD patterns of high-pressure reaction products also showed a more intense (1011) peak compared to the (1010) peak. Our simulations suggest that stacking faults can decrease the intensity ratio of $(10\overline{1}1)$ to $(10\overline{1}0)$ (Figure 5D), and a more intense $(10\overline{1}1)$ peak may imply that WZ-GaN nanocrystals synthesized at high ammonia pressure have fewer stacking faults. GaN nanocrystals synthesized at high ammonia pressure also yielded TEM images of higher contrast compared to the materials synthesized at an ambient pressure (Figure 5B). A PDF analysis further confirmed the formation of highly crystalline GaN (Figure 5E). It is notable that the PDF of GaN nanorods synthesized with high-pressure ammonia exhibits long-range correlations, up to ~7 nm distances (Figure 5F). The period of these oscillations was 0.26

nm, which is one-half of c-lattice constant of GaN, implying elongation of WZ nanocrystals along [0001] direction.

The absorption spectra of colloidal GaN nanorods showed absorption peaks that can be assigned to the excitonic transitions. As the synthesis pressure increased, the excitonic transitions in the absorption spectra of GaN nanorods shifted to longer wavelengths, as expected for reduced quantum confinement for larger nanorod diameters (Figure 6A). Upon excitation at 270 nm, colloidal GaN nanorods synthesized at 5 MPa ammonia pressure showed a broad band of trap emission centered around 580 nm (Figure 6B). The photoluminescence excitation (PLE) spectra confirm that this trap emission originated from the particles. PLE spectra measured at different emission wavelengths indicate that our product consisted of nanocrystals of different absorption profiles and that thicker particles showed redder trap emission.

Colloidal GaN nanoparticle samples often showed a photoluminescence (PL) band between 300 and 350 nm. The solution of GaN nanorods synthesized at 5 MPa ammonia pressure also showed a small peak at 330 nm (Figure 6B and Figure S7A). Very similar ultraviolet (UV) emission components slightly red-shifted with respect to the excitonic absorption peaks were observed in many GaN nanocrystal samples (Figure S7B). These PL peaks are reminiscent of the band-edge emission from radiative exciton recombination, but

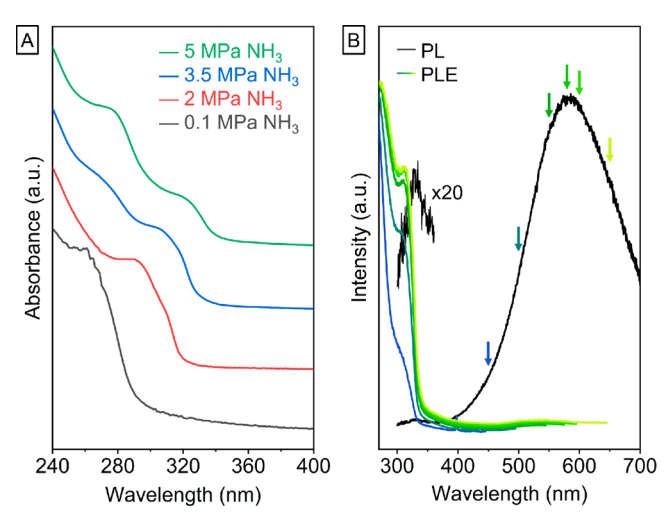


Figure 6. Optical properties of GaN nanorods synthesized using high-pressure ammonia. (A) Absorption spectra of GaN nanorods dispersed in methylcyclohexane produced using different ammonia pressures. Small artifacts between 250 and 270 nm are from trace amounts of residual toluene. (B) Photoluminescence (PL, black curves) and photoluminescence excitation (PLE, colored curves) spectra of GaN nanorods from synthesis with 5 MPa ammonia. Arrows indicate the monitored emission wavelengths of PLE spectra of corresponding colors. The PLE spectra hint that the populations of thicker nanorods emit from midgap states of lower energy.

such an assignment requires great caution because molecular gallium species coordinated with amines and halides can also emit in this wavelength range. For example, we found that a stoichiometric mixture of gallium chloride and oleylamine dissolved in methylcyclohexane showed emission centered around 325 nm upon excitation at 270 nm (Figure S7C). As a small quantity of gallium-amine complexes can be present in colloidal solutions of GaN nanocrystals as impurities, weak band-edge-like emission components of these solutions may be misleading. Similar to other nanocrystal systems, we expect that further improvements of surface passivation of GaN nanocrystals, e.g., by growing core—shell nanoheterostructures, will significantly amplify the band-edge emission.

To the best of our knowledge, controlling ammonia pressure has not previously been used for solution synthesis of III-nitride nanomaterials. We showed that elevated ammonia pressure can be useful for the synthesis of GaN nanocrystals, as their sizes and correspondingly their size-dependent electronic structures due to the quantum confinement effect can be successfully varied by controlling ammonia pressure. Growing nanocrystals with better crystal quality will be beneficial for shell growth and other postsynthetic modifications, film deposition, electronic and optoelectronic properties, as well as other material characteristics.

CONCLUSION

We found that an inclusion of a molten salt phase into solution synthesis enables the formation of crystalline GaN and AlN nanoparticles at mild temperatures. In the case of GaN, nanocrystals with different crystal phases and shapes could be obtained, depending on the precursor. We further showed that high-pressure ammonia increases the diameter of GaN nanorods and improves their crystallinity. We suggest that molten salt phases provide a solvent that is capable of

stabilizing charged species generated during monomer detachment step, which facilitates microscopic reversibility necessary for the growth of defect-free crystals. By utilizing molten salt emulsions, we hope that various III-nitrides and other difficult-to-crystallize materials can be synthesized *via* inexpensive and scalable solution methods for future applications.

METHODS

Chemicals. Aluminum bromide (AlBr₃, Alfa Aesar, ultra dry, 99.999%), ethanol (Sigma-Aldrich, 200 proof, anhydrous, \geq 99.5%), n-hexane (Sigma-Aldrich, anhydrous, 95%), gallium bromide (GaBr₃, Alfa Aesar, ultra dry, 99.998%), gallium chloride (GaCl₃, Alfa Aesar, ultra dry, 99.999%), gallium iodide (GaI3, Alfa Aesar, ultra dry, powder, 99.999%), methanol (Sigma-Aldrich, anhydrous, 99.8%), methylcyclohexane (Sigma-Aldrich, anhydrous, ≥ 99%), potassium chloride (KCl, Alfa Aesar, ultra dry, 99.95%), and toluene (Sigma-Aldrich, anhydrous, 99.8%) were stored under inert atmosphere and used as received. Potassium tetrachlorogallate (KGaCl₄) was prepared by melting a stoichiometric mixture of GaCl₃ and KCl under nitrogen. Oleic acid (Sigma-Aldrich, technical grade, 90%), oleylamine (Sigma-Aldrich, technical grade, 70%), and stearic acid (Fluka, 97%) were dried under a vacuum at 100 °C for 3 h and stored under nitrogen. Trioctylamine (TOA, Sigma-Aldrich, 98%) and hexadecylamine (HDA, Sigma-Aldrich, technical grade, 90%) were vacuum distilled over sodium (Sigma-Aldrich, 99.8%) and stored under nitrogen. Since it is solid at room temperature, HDA was heated gently to melt it before use. Ammonia gas (Airgas, anhydrous grade) was distilled over sodium (Sigma-Aldrich, 99.8%) in a dry ice bath right before use for ambient-pressure syntheses. For high-pressure syntheses, the same ammonia gas was condensed inside a high-pressure vessel. Details about high-pressure setups are described below.

Synthesis of Gallium Oxynitride. A solution of gallium stearate was prepared by degassing 0.5 mmol GaCl₃ and 1.5 mmol of stearic acid in 5 mL of TOA at 90 °C for 3 h under a vacuum with vigorous stirring. After degassing, the solution of gallium stearate was heated to 290 °C under nitrogen. Excess ammonia was passed over this mixture for 5 min. The reaction mixture was then heated for 1 h at 290 °C. After the reaction, the reaction mixture was cooled to a room temperature by removing the heat source. The gallium oxynitride produced was noncolloidal and was separated from the mixture by centrifugation. The obtained solid was washed with toluene, ethanol, and methanol a few times each.

Synthesis of Amorphous GaN and AlN. In a nitrogen atmosphere, 0.5–1 mmol of gallium or aluminum halide was fully dissolved in 4 mL of TOA. To this mixture, 0.6 g of HDA was added. For heating-up syntheses, the mixture was heated to 290 °C under constant ammonia flow with vigorous stirring. Alternatively, for hotinjection synthesis, the mixture was heated to 290 °C under nitrogen, and then, ammonia was passed over the solution for 5 min. In both cases, the reaction mixture was heated afterward for 1 h at 290 °C. The reaction mixture was cooled to a room temperature by removing the heat source. White solids precipitated from the reaction mixture upon cooling. This solid was separated from the solution by centrifugation and washed with 10 mL of toluene a few times for the removal of excess organic materials. The remaining solids were washed with 40 mL of methanol a few times to remove ammonium halide byproducts of the reaction.

Synthesis of Crystalline GaN and AlN with Ambient-Pressure Ammonia. In a nitrogen atmosphere, 5 mmol of finely ground gallium or aluminum halide salt was mixed with 4 mL of TOA and 0.6 g of HDA. In a typical heat-up synthesis, the mixture was heated to 290 °C under constant ammonia flow with vigorous stirring. For the KGaCl₄ control experiment, the reaction mixture was first heated to 290 °C, and then, ammonia was passed over the solution for 5 min. After 1 h of heating at 290 °C, the heat source was removed, and the reaction mixture was cooled to room temperature. The product spontaneously precipitated from the reaction mixture. This solid was separated with centrifugation, and washed first with 10 mL of toluene and then with 40 mL of methanol a few times each to

remove excess organics and salt byproducts. To extract colloidal particles from the solid, the solid was sonicated for 30 min with the mixture of 16 mL of n-hexane (or toluene), 2 mL of oleylamine, and 2 mL of oleic acid. A solution of nanoparticles was separated with centrifugation from noncolloidal solid. From this solution, nanoparticles could be flocculated with ethanol. Particles were washed a few times with ethanol before finally dispersed in methylcyclohexane or n- hexane for measurements.

High-Pressure Setup. Two identical high-pressure vessels from Parr Instrument Company (Series 4740, 75 mL) were used for the setup (Figure S9). A tee with three needle valves was set to connect two vessels and a Schlenk line, which was necessary to operate the system under air-free conditions. To one fully evacuated vessel, liquid ammonia was condensed by using an ice/water bath. The other one, equipped with a silicon nitride liner and a needle valve, worked as a detachable reaction vessel, which could be brought in and out of the nitrogen glovebox for air-free preparation of the reaction mixture. For an operation, the system was assembled and properly evacuated through a Schlenk line. Two heating tapes were used to heat the two vessels separately. Caution! The pressure of ammonia will be high enough to break glassware, so needle valves must be manipulated with care to ensure high-pressure ammonia is not admitted to the Schlenk line.

Synthesis of GaN under High-Pressure Ammonia. In the reaction vessel, 5 mmol of finely ground KGaCl₄, 4 mL of TOA, and 0.6 g of HDA were loaded together with a glass stirbar under nitrogen atmosphere. After the reaction vessel was assembled to the system, two pressure vessels were heated separately; the one with the reaction mixture was heated to 290 °C under ambient pressure nitrogen with vigorous stirring, while the other with liquid ammonia was heated gently to a pressure about 2-3 MPa higher than the target pressure. To the heated reaction mixture, the desired pressure (2, 3.5, or 5 MPa) of hot ammonia gas was transferred by manipulating the two needle valves between the two pressure vessels. During this process, the needle valve toward the Schlenk line must be closed. After 1 h of reaction, pressurized gas in the reaction vessel was slowly vented until the pressure reached 1 MPa, a pressure high enough to prevent back flow of an air into the vessel during venting and low enough to avoid a condensation of liquid ammonia during cooling. The reaction vessel was cooled to a room temperature and transferred into a nitrogen atmosphere. The reaction product was washed with toluene and methanol a few times each. Colloidal solutions of these products were obtained by sonication of the solid products with 16 mL of *n*-hexane (or toluene), 2 mL of oleylamine, and 2 mL of oleic acid. Nanoparticles were flocculated with ethanol from this solution, collected by centrifugation, and dispersed in methylcyclohexane or nhexane for subsequent measurements.

Characterization Techniques. Transmission Electron Microscopy (TEM). TEM images were obtained with a 300 kV FEI Tecnai G2 F30 microscope. Samples were prepared by drying colloidal solutions diluted in toluene on Ted Pella pure carbon film grids. After evaporation of toluene, grids were washed gently with ethanol and dried under a vacuum. As the lattice contrast of GaN and AlN nanoparticles in TEM images is naturally low due to low nuclear charges of the materials, small sizes of the nanoparticles, and high accelerating voltage of electron beam source, for better visibility, lattice fringes in high-resolution TEM images were enhanced in contrast with Gatan DigitalMicrograph. Details of this enhancement procedure are given in the Supporting Information.

Optical Spectra. Colloidal samples were gently washed with ethanol to remove excess organic ligands and the original solvent and then were redispersed as dilute solutions in methylcyclohexane. Absorption spectra of these solution samples were taken with a Shimadzu UV-3600 Plus spectrophotometer from 220 to 500 nm. Photoluminescence (PL) and photoluminescence excitation (PLE) spectra of solution samples were taken with a Horiba Jobin Yvon FluoroMax-4.

Powder X-ray Diffraction (PXRD). PXRD patterns were obtained with a Rigaku MiniFlex with a Cu K α source. Samples were prepared by drying concentrated colloidal solutions on zero-diffraction silicon plates (Rigaku 906165 Flush, Si510).

Pair Distribution Function (PDF) Measurement. PDF data was collected from beamline 11-ID-B of the Advanced Photon Source (APS) at Argonne National Laboratory (ANL). Total scattering data were acquired as images on a large flat panel detector. GSAS-II software⁵⁴ was used to reduce 2D diffraction images to 1D diffraction patterns. Masks were drawn and integration processes were carried out using the GSAS-II software. Pair distribution functions were extracted from 1D diffraction patterns in the q range of $0.1-23.1 \text{ Å}^{-1}$.

ASSOCIATED CONTENT

Supporting Information

The Supporting Information is available free of charge at https://pubs.acs.org/doi/10.1021/acsnano.2c09552.

Discussions of simulation details and figures of PXRD patterns, TEM image of GaN nanocrystal from GaBr₃, PDFs of GaN nanocrystals, images of biphasic and monophasic mixtures of gallium salts and amines, optical spectra of GaN nanocrystals and gallium-hallide-amine complex, details on TEM image contrast enhancement, and scheme for a high-pressure reactor system (PDF)

AUTHOR INFORMATION

Corresponding Author

Dmitri V. Talapin – Department of Chemistry, James Franck Institute, and Pritzker School of Molecular Engineering, University of Chicago, Chicago, Illinois 60637, United States; Center for Nanoscale Materials, Argonne National Laboratory, Argonne, Illinois 60517, United States; orcid.org/0000-0002-6414-8587; Email: dvtalapin@ uchicago.edu

Authors

Wooje Cho - Department of Chemistry, James Franck Institute, and Pritzker School of Molecular Engineering, University of Chicago, Chicago, Illinois 60637, United States; orcid.org/0000-0002-4022-4194

Zirui Zhou - Department of Chemistry, James Franck Institute, and Pritzker School of Molecular Engineering, University of Chicago, Chicago, Illinois 60637, United States

Ruiming Lin - Department of Chemistry, James Franck Institute, and Pritzker School of Molecular Engineering, University of Chicago, Chicago, Illinois 60637, United States

Justin C. Ondry – Department of Chemistry, James Franck Institute, and Pritzker School of Molecular Engineering, University of Chicago, Chicago, Illinois 60637, United States; orcid.org/0000-0001-9113-3420

Complete contact information is available at: https://pubs.acs.org/10.1021/acsnano.2c09552

Notes

The authors declare no competing financial interest.

ACKNOWLEDGMENTS

The authors thank Dr. Andrew Nelson (University of Chicago) for a critical reading of the manuscript, Dr. Leighanne C. Gallington (Advanced Photon Source, ANL) for helping with PDF measurements, and Dr. V. Petkov (Central Michigan University) for sharing his X-ray PDF data. The work on GaN and AlN nanomaterials synthesis in molten salt media was supported by the National Science Foundation under award number DMR-2004880. Advanced characterization of nanomaterials and colloidal dispersions was supported by the Center for Hierarchical Materials Design (CHiMad) supported

by U.S. Department of Commerce, National Institute of Standards and Technology under financial assistance award number 70NANB14H012. Modeling and simulations were supported by MICCoM, as part of the Computational Materials Sciences Program funded by the US Department of Energy, Office of Science, BES, Materials Sciences and Engineering Division under Award 5J-30161-0010A. This work used resources from the Center for Nanoscale Materials, a U.S. Department of Energy (DOE) Office of Science User Facility operated for the DOE Office of Science by Argonne National Laboratory under Contract no. DE-AC02-06CH11357. This research also used resources of the Advanced Photon Source, a U.S. Department of Energy (DOE) Office of Science User Facility operated for the DOE Office of Science by Argonne National Laboratory under Contract No. DE-AC02-06CH11357. The mail-in program at Beamline 11-ID-B contributed to the data reposted in this work.

REFERENCES

- (1) Nakamura, S.; Mukai, T.; Senoh, M.; Iwasa, N. Thermal Annealing Effects on P-Type Mg-Doped GaN Films. *Jpn. J. Appl. Phys.* **1992**, 31, L139–L142.
- (2) Ding, X.; Zhou, Y.; Cheng, J. A Review of Gallium Nitride Power Device and Its Applications in Motor Drive. CES trans. electr. mach. syst. 2019, 3, 54–64.
- (3) Oda, O. Nitride and Other III-V Compounds. *Compound Semiconductor Bulk Materials and Characterizations*; World Scientific Publishing Co.: Singapore, 2012; Vol. 2, pp 27–125.
- (4) Raty, J.-Y.; Schumacher, M.; Golub, P.; Deringer, V. L.; Gatti, C.; Wuttig, M. A Quantum-Mechanical Map for Bonding and Properties in Solids. *Adv. Mater.* **2019**, *31*, 1806280.
- (5) Iqbal, A.; Mohd-Yasin, F. Reactive Sputtering of Aluminum Nitride (002) Thin Films for Piezoelectric Applications: A Review. *Sensors* **2018**, *18*, 1797.
- (6) Liu, G.; Zhou, G.; Qin, Z.; Zhou, Q.; Zheng, R.; Wu, H.; Sun, Z. Luminescence Characterizations of Freestanding Bulk Single Crystalline Aluminum Nitride towards Optoelectronic Application. *CrystEngComm* **2017**, *19*, 5522–5527.
- (7) Lu, T.-J.; Fanto, M.; Choi, H.; Thomas, P.; Steidle, J.; Mouradian, S.; Kong, W.; Zhu, D.; Moon, H.; Berggren, K.; Kim, J.; Soltani, M.; Preble, S.; Englund, D. Aluminum Nitride Integrated Photonics Platform for the Ultraviolet to Visible Spectrum. *Opt. express* **2018**, *26*, 11147–11160.
- (8) Bondokov, R. T.; Mueller, S. G.; Morgan, K. E.; Slack, G. A.; Schujman, S.; Wood, M. C.; Smart, J. A.; Schowalter, L. J. Large-Area AlN Substrates for Electronic Applications: An Industrial Perspective. *J. Cryst. Growth* **2008**, *310*, 4020–4026.
- (9) Piazza, G.; Stephanou, P. J.; Pisano, A. P. Piezoelectric Aluminum Nitride Vibrating Contour-Mode MEMS Resonators. J. Microelectromech. Syst. 2006, 15, 1406–1418.
- (10) Bhattacharyya, A.; Moustakas, T.; Zhou, L.; Smith, D. J.; Hug, W. Deep Ultraviolet Emitting AlGaN Quantum Wells with High Internal Quantum Efficiency. *Appl. Phys. Lett.* **2009**, *94*, 181907.
- (11) Jones, A. C.; Whitehouse, C. R.; Roberts, J. S. Chemical Approaches to the Metalorganic CVD of Group-III Nitrides. *Chem. Vap. Deposition* **1995**, *1*, 65–74.
- (12) Richter, T. M.; Niewa, R. Chemistry of Ammonothermal Synthesis. *Inorganics* **2014**, *2*, 29–78.
- (13) Han, W.; Fan, S.; Li, Q.; Hu, Y. Synthesis of Gallium Nitride Nanorods through a Carbon Nanotube-Confined Reaction. *Science* **1997**, 277, 1287–1289.
- (14) Goldberger, J.; He, R.; Zhang, Y.; Lee, S.; Yan, H.; Choi, H.-J.; Yang, P. Single-Crystal Gallium Nitride Nanotubes. *Nature* **2003**, 422, 599–602.
- (15) Tang, Y.; Cong, H.; Zhao, Z.; Cheng, H. Field Emission from AlN Nanorod Array. Appl. Phys. Lett. 2005, 86, 153104.

- (16) Shen, L.; Lv, W.; Wang, N.; Wu, L.; Qi, D.; Ma, Y.; Lei, W. Controllable Synthesis of AlN Nanostructures and Their Photoluminescence. *CrystEngComm* **2017**, *19*, 5940–5945.
- (17) Lei, W.; Liu, D.; Zhang, J.; Zhu, P.; Cui, Q.; Zou, G. Direct Synthesis, Growth Mechanism, and Optical Properties of 3D AlN Nanostructures with Urchin Shapes. *Cryst. Growth Des.* **2009**, *9*, 1489–1493.
- (18) Zhang, F.; Wu, Q.; Wang, X.; Liu, N.; Yang, J.; Hu, Y.; Yu, L.; Wang, X.; Hu, Z.; Zhu, J. 6-Fold-Symmetrical AlN Hierarchical Nanostructures: Synthesis and Field-Emission Properties. *J. Phys. Chem. C* **2009**, *113*, 4053–4058.
- (19) Chen, F.; Ji, X.; Lau, S. P. Recent Progress in Group III-Nitride Nanostructures: From Materials to Applications. *Mater. Sci. Eng. R Rep.* **2020**, *142*, 100578.
- (20) Al Balushi, Z. Y.; Wang, K.; Ghosh, R. K.; Vilá, R. A.; Eichfeld, S. M.; Caldwell, J. D.; Qin, X.; Lin, Y.-C.; DeSario, P. A.; Stone, G.; Subramanian, S.; Paul, D. F.; Wallace, R. M.; Datta, S.; Redwing, J. M.; Robinson, J. A. Two-Dimensional Gallium Nitride Realized via Graphene Encapsulation. *Nat. Mater.* **2016**, *15*, 1166–1171.
- (21) Chen, Y.; Liu, K.; Liu, J.; Lv, T.; Wei, B.; Zhang, T.; Zeng, M.; Wang, Z.; Fu, L. Growth of 2D GaN Single Crystals on Liquid Metals. *J. Am. Chem. Soc.* **2018**, *140*, 16392–16395.
- (22) Wang, Y.; Fedin, I.; Zhang, H.; Talapin, D. V. Direct Optical Lithography of Functional Inorganic Nanomaterials. *Science* **2017**, 357, 385–388.
- (23) Sardar, K.; Rao, C. New Solvothermal Routes for GaN Nanocrystals. *Adv. Mater.* **2004**, *16*, 425–429.
- (24) Choi, Y. C.; Kim, H.; Lee, C.; Son, J.; Baik, H.; Park, S.; Kim, J.; Jeong, K. S. Blue Emission of α -GaN Colloidal Quantum Dots via Zn Doping. *Chem. Mater.* **2019**, *31*, 5370–5375.
- (25) Manz, A.; Birkner, A.; Kolbe, M.; Fischer, R. A. Solution Synthesis of Colloidal Gallium Nitride at Unprecedented Low Temperatures. *Adv. Mater.* **2000**, *12*, 569–573.
- (26) Mićić, O.; Ahrenkiel, S.; Bertram, D.; Nozik, A. J. Synthesis, Structure, and Optical Properties of Colloidal GaN Quantum Dots. *Appl. Phys. Lett.* **1999**, *75*, 478–480.
- (27) Pan, G.; Kordesch, M. E.; Van Patten, P. G. New Pyrolysis Route to GaN Quantum Dots. *Chem. Mater.* **2006**, *18*, 3915–3917.
- (28) Lan, Y.; Chen, X.; Cao, Y.; Xu, Y.; Xun, L.; Xu, T.; Liang, J. Low-Temperature Synthesis and Photoluminescence of AlN. *J. Cryst. Growth* **1999**, 207, 247–250.
- (29) Sardar, K.; Rao, C. AlN Nanocrystals by New Chemical Routes. *Solid State Sci.* **2005**, *7*, 217–220.
- (30) Lu, S.; Tong, Y.; Liu, Y.; Xu, C.; Lu, Y.; Zhang, J.; Shen, D.; Fan, X. The Structure and Optical Properties of AlN Nanocrystals Prepared by Schlenk Techniques at Atmospheric Pressure and Low Temperature. *J. Phys. Chem. Solids* **2005**, *66*, 1609–1613.
- (31) Whitelam, S.; Jack, R. L. The Statistical Mechanics of Dynamic Pathways to Self-Assembly. *Annu. Rev. Phys. Chem.* **2015**, *66*, 143–163
- (32) Luo, Y.-R.; Kerr, J. A. Bond Dissociation Energies. In *CRC Handbook of Chemistry and Physics*, 87th ed.; Lide, D. R., Ed.; CRC Press/Talyor and Francis: Boca Raton, FL, 2006.
- (33) Kandalam, A. K.; Pandey, R.; Blanco, M.; Costales, A.; Recio, J.; Newsam, J. M. First Principles Study of Polyatomic Clusters of AlN, GaN, and InN. 1. Structure, Stability, Vibrations, and Ionization. *J. Phys. Chem. B* **2000**, *104*, 4361–4367.
- (34) Herndon, L. R.; Reid, E. E. The Decomposition of Organic Compounds at High Temperatures and Pressures. *J. Am. Chem. Soc.* **1928**, *50*, 3066–3073.
- (35) Riedinger, A.; Ott, F. D.; Mule, A.; Mazzotti, S.; Knüsel, P. N.; Kress, S. J.; Prins, F.; Erwin, S. C.; Norris, D. J. An Intrinsic Growth Instability in Isotropic Materials Leads to Quasi-Two-Dimensional Nanoplatelets. *Nat. Mater.* **2017**, *16*, 743–748.
- (36) Reiss, P.; Carriere, M.; Lincheneau, C.; Vaure, L.; Tamang, S. Synthesis of Semiconductor Nanocrystals, Focusing on Nontoxic and Earth-Abundant Materials. *Chem. Rev.* **2016**, *116*, 10731–10819.

- (37) Fan, G.; Wang, C.; Fang, J. Solution-Based Synthesis of III-V Quantum Dots and Their Applications in Gas Sensing and Bio-Imaging. *Nano Today* **2014**, *9*, 69–84.
- (38) Ramasamy, P.; Kim, N.; Kang, Y.-S.; Ramirez, O.; Lee, J.-S. Tunable, Bright, and Narrow-Band Luminescence from Colloidal Indium Phosphide Quantum Dots. *Chem. Mater.* **2017**, *29*, 6893–6899
- (39) Battaglia, D.; Peng, X. Formation of High Quality InP and InAs Nanocrystals in a Noncoordinating Solvent. *Nano Lett.* **2002**, *2*, 1027–1030.
- (40) Gates-Rector, S.; Blanton, T. The Powder Diffraction File: A Quality Materials Characterization Database. *Powder Diffr.* **2019**, 34, 352–360.
- (41) Yu, M.; Drabold, D. Density Dependence of the Structural and Electronic Properties of Amorphous GaN. *Solid State Commun.* **1998**, 108, 413–417.
- (42) Waggoner, K. M.; Olmstead, M. M.; Power, P. P. Structural and Spectroscopic Characterization of the Compounds [Al(NMe2)3]2, [Ga(NMe2)3]2, [(Me2N)2Al{ μ -N(H)1-Ad}]2 (1-Ad = 1-Adamantanyl) and [{Me(μ -NPh2)Al}2NPh(μ -C6H4)]. Polyhedron **1990**, 9, 257–263.
- (43) Anderson, N. C.; Hendricks, M. P.; Choi, J. J.; Owen, J. S. Ligand Exchange and the Stoichiometry of Metal Chalcogenide Nanocrystals: Spectroscopic Observation of Facile Metal-Carboxylate Displacement and Binding. *J. Am. Chem. Soc.* **2013**, *135*, 18536–18548
- (44) Dumbgen, K. C.; Zito, J.; Infante, I.; Hens, Z. Shape, Electronic Structure, and Trap States in Indium Phosphide Quantum Dots. *Chem. Mater.* **2021**, 33, 6885–6896.
- (45) Bugaris, D. E.; zur Loye, H. C. Materials Discovery by Flux Crystal Growth: Quaternary and Higher Order Oxides. *Angew. Chem., Int. Ed.* **2012**, *51*, 3780–3811.
- (46) Gupta, S. K.; Mao, Y. Recent Developments on Molten Salt Synthesis of Inorganic Nanomaterials: A Review. *J. Phys. Chem. C* **2021**, *125*, 6508–6533.
- (47) Wiley, J. B.; Kaner, R. B. Rapid Solid-State Precursor Synthesis of Materials. *Science* **1992**, *255*, 1093–1097.
- (48) Treece, R. E.; Macala, G. S.; Rao, L.; Franke, D.; Eckert, H.; Kaner, R. B. Synthesis of III-V Semiconductors by Solid-State Metathesis. *Inorg. Chem.* **1993**, 32, 2745–2752.
- (49) Cunningham, P. D.; Coropceanu, I.; Mulloy, K.; Cho, W.; Talapin, D. V. Quantized Reaction Pathways for Solution Synthesis of Colloidal ZnSe Nanostructures: A Connection between Clusters, Nanowires, and Two-Dimensional Nanoplatelets. *ACS Nano* **2020**, 14, 3847–3857.
- (50) Manna, L.; Scher, E. C.; Alivisatos, A. P. Synthesis of Soluble and Processable Rod-, Arrow-, Teardrop-, and Tetrapod-Shaped CdSe Nanocrystals. *J. Am. Chem. Soc.* **2000**, *122*, 12700–12706.
- (51) DuChene, J. S.; Niu, W.; Abendroth, J. M.; Sun, Q.; Zhao, W.; Huo, F.; Wei, W. D. Halide Anions as Shape-Directing Agents for Obtaining High-Quality Anisotropic Gold Nanostructures. *Chem. Mater.* **2013**, 25, 1392–1399.
- (52) Filankembo, A.; Giorgio, S.; Lisiecki, I.; Pileni, M. Is the Anion the Major Parameter in the Shape Control of Nanocrystals? *J. Phys. Chem. B* **2003**, *107*, 7492–7500.
- (53) Ehrentraut, D.; Kagamitani, Y. Acidic Ammonothermal Growth Technology for GaN. *Technology of Gallium Nitride Crystal Growth*; Springer-Verlag Berlin Heidelberg: Berlin, Heidelberg, 2010; pp 183–203.
- (54) Toby, B. H.; Von Dreele, R. B. Gsas-II: The Genesis of a Modern Open-Source All Purpose Crystallography Software Package. *J. Appl. Crystallogr.* **2013**, *46*, 544–549.

☐ Recommended by ACS

Synthesis of Size-Tunable Indium Nitride Nanocrystals

Dingchen Wen, Paul Mulvaney, et al.

APRIL 10, 2023

THE JOURNAL OF PHYSICAL CHEMISTRY LETTERS

READ 🗹

High-Frequency EPR and ENDOR Spectroscopy of Mn²⁺ Ions in CdSe/CdMnS Nanoplatelets

Roman A. Babunts, Pavel G. Baranov, et al.

FEBRUARY 20, 2023

ACS NANO

RFAD 🗹

Colloidal Ternary Telluride Quantum Dots for Tunable Phase Change Optics in the Visible and Near-Infrared

Dhananjeya Kumaar, Maksym Yarema, et al.

MARCH 27, 2023

ACS NANO

READ 🗹

Red Emission from Copper-Vacancy Color Centers in Zinc Sulfide Colloidal Nanocrystals

Sarah M. Thompson, Cherie R. Kagan, et al.

MARCH 09, 2023

ACS NANO

READ 🗹

Get More Suggestions >